Role of spins in molecular photoionization: Spectroscopy and dynamics of autoionizing Rydberg states of ortho-H_2

H. J. Wörner,[1] S. Mollet,[1] Ch. Jungen,[2] and F. Merkt[1]

[1]*Laboratorium für Physikalische Chemie, ETH-Zürich, 8093 Zürich, Switzerland*

[2]*Laboratoire Aimé-Cotton du CNRS, Université de Paris-Sud, 91405 Orsay Cédex, France*

A combined experimental and theoretical investigation of the role of electronic and nuclear spins in molecular photoionization is reported. Photoionization spectra of autoionizing p Rydberg states belonging to series converging on the X $^2\Sigma_g^+(v^+=0, N^+=3)$ level of ortho-H_2^+ have been measured in the range of principal quantum number $n=50$–200 from the long-lived H $^1\Sigma_g^+(v=0, J=3)$ level. The use of a pulsed near-Fourier-transform-limited laser with a bandwidth of less than 10 MHz resulted in a Doppler-limited linewidth of 25 MHz which sufficed to partially resolve the hyperfine structure of the Rydberg states. Below $n \approx 70$, the exchange interaction between the ion core and Rydberg electrons is larger than the hyperfine interactions in the ion core and the observed levels can be understood in terms of Hund's angular momentum coupling case (d). With increasing value of n, the hyperfine interactions in the core lead to a mixing of singlet and triplet characters of the Rydberg states and eventually to a complete decoupling of the Rydberg electron spin from the core spins that results in distinct series converging on the hyperfine components of the ion. Several intermediate coupling cases have been identified and two of them completely characterized. Most interestingly, the total spin angular momentum has been found to be a good quantum number up to $n \approx 150$ at least, i.e., far beyond the region where the ionic hyperfine structure starts dominating the coupling hierarchy. Multichannel quantum defect theory including nuclear and electron spins has been extended to treat autoionization and predict spectral intensities. The comparison with the experimental spectra has revealed a satisfactory agreement between calculated and measured line positions, linewidths, and intensities and has enabled us to extract, by extrapolation, a more accurate term value for the H $^1\Sigma_g^+(v=0, J=3)$ level. The calculations have been used to characterize the role of hyperfine, spin-rotational, and pf interactions in rotational autoionization and have revealed a very strong dependence of the autoionization lifetimes of high Rydberg states on the value of the total angular momentum quantum number F.

PACS number(s): 33.15.Pw, 33.80.Eh, 33.80.Rv, 31.10.+z

I. INTRODUCTION

Photoionization spectra of atoms and molecules are an important source of structural and dynamical information on these systems. In the vicinity of the first adiabatic ionization energy, molecular photoionization spectra are characterized by a rich structure originating from the autoionization of Rydberg states belonging to series converging on vibrational and rotational levels of the cation [1,2]. The autoionization dynamics can be described in terms of interaction parameters between the different ionization channels [3,4] but a complete understanding of the rovibrational channel interactions has so far only been reached in prototypical molecular systems, primarily H_2 [5–8].

Multichannel quantum defect theory (MQDT) provides the basis for the description of the underlying mechanisms and permits a unified treatment of bound and autoionizing Rydberg series and the associated ionization continua. Current research in molecular photoionization and MQDT is oriented in two main directions: On the one hand, the formalism that has been so successfully developed and used to describe the rovibronic photoionization dynamics of H_2 is increasingly applied to model the photoionization dynamics of larger molecules such as CaF [9] or N_2 [10] and tri- and tetraatomic molecules (H_2O [11–14], HCO [15,16], NH_3 [17]). On the other hand, the first spectra have been reported in which the hyperfine structure of bound and autoionizing Rydberg states could be resolved [18–21]. The analysis of

such spectra requires the inclusion of nuclear spins into the formalism of MQDT and recent examples include the analysis of bound Rydberg states of ^{83}Kr [18,22] and ortho-H_2 [19,21] and the study of the effects of nuclear spins on the autoionization dynamics of Rydberg states of ^{129}Xe and ^{131}Xe [20]. In each case, the extrapolation of the observed structures could be used to derive the hyperfine structure of the ions [18–20,22].

The present paper describes the results of a joint experimental and theoretical investigation of the role of nuclear spins in the autoionization of Rydberg series converging on the first rotationally excited level of ortho H_2^+ (X $^2\Sigma_g^+$, $v^+=0$, $N^+=3$). Experimentally, these Rydberg states were accessed from the $v=0$, $J=3$ level of the H $^1\Sigma_g^+$ state of H_2 using a narrow-band (bandwidth <10 MHz) solid-state near-infrared laser [23,24]. The H $^1\Sigma_g^+(v=0, J=3)$ level was chosen because its lifetime ($\tau=102$ ns [25]) is much longer than that of singlet ungerade levels [0.5 ns [26] for B $^1\Sigma_u^+(v=0, J=0)$]. The experimental resolution of down to 25 MHz enabled the observation of the fine and hyperfine structures of the autoionizing Rydberg states over a wide range of principal quantum number $n=50$–200. The spectra provide information on previously unknown dynamical processes related to nuclear spins and reveal the evolution of angular momentum coupling hierarchy from the situation where the exchange interaction dominates the level structure to the situation where the ionic hyperfine structure dominates. Several intermediate angular momentum coupling cases are identified

which are useful in rationalizing both the level structure and the autoionization dynamics. An essential result is the observation that the total spin remains a conserved quantity in photoexcitation. Theoretically, the MQDT formalism developed to treat the hyperfine structure of bound Rydberg states of diatomic molecules [19,21] has been extended to also describe the hyperfine structure and dynamics of autoionizing Rydberg states. The calculations permit the exploration and quantification of phenomena not observed in the present experiment such as spin-induced autoionization.

This article is structured as follows. Section II provides a short description of the experimental procedure. The MQDT formalism describing the hyperfine structure of autoionizing Rydberg states of H_2 is presented in Sec. III. Section IV provides an analysis of the observed spectra and a comparison with the predictions of MQDT. We discuss in particular the evolution of the angular momentum coupling hierarchy and establish that the total spin quantum number G is conserved in photoexcitation over the whole range of observed spectra. In Sec. V the autoionization processes induced by the electron and nuclear spins are discussed and rationalized.

II. EXPERIMENT

The spectra have been recorded using sources of tunable vacuum-ultraviolet (vuv), visible (vis), and near-infrared (nir) laser radiation. The following three-photon excitation sequence was used to excite the high-n p Rydberg states of ortho-H_2 below the $X \, ^2\Sigma_g^+$ $(v^+=0, N^+=3)$ ionization threshold:

$$X(v = 0, J = 1, F = 0 - 2),$$

$$\overset{\text{vuv}}{\rightarrow} B(v = 5, J = 2, F = 1 - 3),$$

$$\overset{\text{vis}}{\rightarrow} H(v = 0, J = 3, F = 2 - 4),$$

$$\overset{\text{nir}}{\rightarrow} np(v^+ = 0, N^+ = 3, N = 2 - 4, F = 1 - 5). \quad (1)$$

This excitation sequence is represented schematically in Fig. 1.

The H_2 sample was introduced into the spectrometer in a skimmed supersonic expansion. The excitation was detected by monitoring the ionization signal resulting from photoionization or pulsed field ionization (PFI) of the long-lived Rydberg states. The accuracy of the reported intensities does not exceed the 20% level because of intensity fluctuations of the laser beams. Because we detect H_2^+ ions for both PFI and photoionization their detection efficiency is identical to an excellent approximation. Ortho-H_2 was selected by fixing the wave number of the vuv laser to the $R(1)$ line of the $B \leftarrow X$ transition.

vuv radiation around 96 400 cm^{-1} was generated by two-photon resonance-enhanced sum-frequency mixing ($\nu_{\text{vuv}} = 2\nu_1 + \nu_2$) of the output of two Nd:YAG-pumped dye lasers in Xe using the $(5p)^5 6p[1/2]_0 \leftarrow (5p)^6 \, ^1S_0$ two-photon resonance at $2\tilde{\nu}_1 = 80118.964$ cm^{-1}. The vuv radiation was sepa-
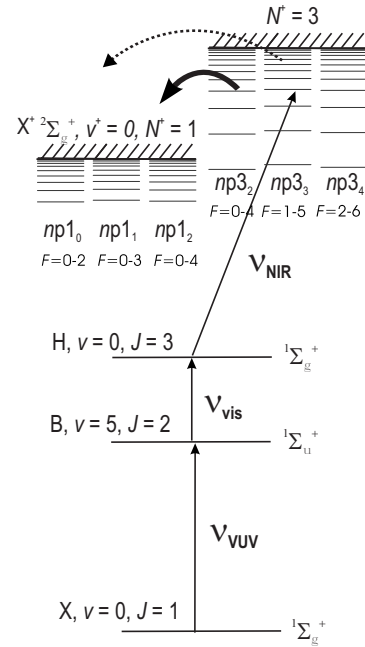

FIG. 1. Schematic energy level diagram representing the resonant three-photon excitation sequence used to excite the Rydberg series converging on the $X \, ^2\Sigma_g^+$, $v^+=0$, $N^+=3$ rotationally excited level of H_2^+. The Rydberg series are designated with the Hund's case (d) labels $n\ell N_N^+$ and the possible values of the total angular momentum quantum number including spins (F). The thick bent arrow represents rotational autoionization allowed in the absence of hyperfine and pf interactions and the dotted arrow represent autoionization that is permitted by hyperfine interactions. The latter affects the $F=1-4$ components of the $np3_3$ and $np3_4$ series.

rated from the fundamental beams in a vacuum monochromator using a toroidal dispersion grating which also recollimated the diverging vuv beam and redirected it toward a photoexcitation-photoionization chamber where it intersected the molecular beam at right angles. The visible radiation was produced by a third dye laser pumped by the same Nd:YAG laser and intersected the vuv beam and the molecular beam at right angles. The pulse energy of this laser had to be attenuated to below 1 μJ in order to prevent undesired two-photon ionization of the B state via the H state. In addition, the size of the laser beam was reduced to 0.2 mm in the direction perpendicular to the molecular beam by a cylindrical lens in order to reduce Doppler broadening. The nir radiation was produced by pulse amplifying the output of a titanium sapphire (Ti:sapphire) ring laser in a multipass bowtie arrangement as described in Ref. [23]. The cw radiation from a Coherent 899-21 Ti:sapphire ring laser was directed into an acousto-optical modulator which was programmed to transmit pulses with a rectangular time profile of adjustable duration. Ten passes through a Nd:YAG-pumped Ti:sapphire crystal yielded pulses of 50 μJ energy with adjustable pulse lengths between 100 and 300 ns and a near Fourier-transform-limited bandwidth of better than 10 MHz. This nir laser beam was directed into the experimental chamber, counterpropagating relative to the vuv laser beam. The overlap of the three laser beams and the molecular beam was optimized by maximizing the ionization signal. The nir ra-

TABLE I. Error budget of the experiment.

Error source	Estim. max. error (MHz)	
Absolute errors		
Frequency calibration	60	stat.
Doppler shift	2	syst.
ac Stark shift	negligible[a]	
dc Stark shift	negligible[b]	syst.
Pressure shift	1	syst.
Chirp shift	5	syst.
Relative errors		
Scan linearization	3	stat.
dc Stark shift	negligible[b]	

[a]All pulse intensities <10 W/mm^2.
[b]For $n<160$ and $\eta>0.06$.

diation was calibrated by (1) recording absorption spectra of molecular iodine in an oven heated to 570 °C, (2) recording the transmission spectrum of a home-built étalon (see below), and (3) by using a wave meter (Burleigh EXFO WA-1500) with an absolute accuracy of 60 MHz.

The error budget of the present measurements of transition frequencies from the H $(v=0,J=3)$ level to high Rydberg states located in the vicinity of the $N^+=3$ ionization threshold is summarized in Table I. The uncertainty in the determination of the transition frequencies is dominated by the accuracy of the frequency calibration. The scans were linearized by using simultaneously recorded transmission spectra of a homebuilt confocal étalon with a free spectral range of 150.08(3) MHz actively locked to a frequency-stabilized HeNe laser [27]. The linearization procedure resulted in a relative frequency uncertainty of at most 3 MHz over the total length of 15 GHz of each scan. For the laser intensities used in this work, ac Stark shifts and broadenings are negligible. The Doppler shift resulting from a possible deviation from 90° of the angle between the nir and molecular beams was measured by recording the same transitions in expansions of pure H$_2$ [beam velocity 2900(50) m s^{-1}], a 1:7 H$_2$:Ar mixture [beam velocity 550(10) m s^{-1}] and a 1:7 H$_2$:Kr mixture [beam velocity 380(10) m s^{-1}]. The Doppler shift was determined with an accuracy of 2 MHz by extrapolating the observed Doppler shifts to zero velocity, the high accuracy resulting from the fact that the Doppler shifts in the three mixtures could be determined relative to the same transmission maximum of the stabilized étalon which remained locked throughout the procedure. At the density of the molecular beam of less than 10^{14} cm^{-3} in the measurement volume, the pressure shift is negligible (i.e., <1 MHz) assuming that the pressure shift measured at $n=10$ [28] can be extrapolated to the high n region. On the basis of the measured residual stray electric fields of less than 2 mV/cm (determined following the procedure described in Ref. [29]), dc Stark shifts can be neglected for Rydberg states with n below 160 and an effective quantum defect of more than 0.06, for which the Stark effect is quadratic. A possible shift of the laser frequency resulting from a chirp occurring in the

nir pulse generation was measured to be less than 5 MHz [23].

Assuming a velocity of the H$_2$ beam of 2900 m s^{-1} and an opening angle of the supersonic beam of 0.3°, a Doppler broadening of 32 MHz is expected at a transition wave number of 11 400 cm^{-1}. The <10 MHz bandwidth of the nir laser thus makes a negligible contribution to the observed linewidth. The Doppler broadening could be decreased by seeding H$_2$ in Kr at a ratio of 1:7, which allowed us to measure a few transitions with a linewidth of 25 MHz or 0.0008 cm^{-1}. The narrowest lines observed experimentally still reveal a partially resolved substructure which eventually limits the observed linewidth. This observation is confirmed by the calculations presented in Sec. IV that predict each observed line to consist of at least three transitions corresponding to different values of the total angular momentum quantum number F.

III. THEORY

The hyperfine structure of bound Rydberg states of ortho-H$_2$ has been studied previously by MQDT as described in Refs. [19,21] which contain the essential equations. We discuss here how these equations are adapted to autoionizing Rydberg states and introduce the equations for the calculation of spectral intensities.

The quantization condition for bound Rydberg levels is obtained by requiring that the wave function vanishes for an infinite distance r between the ion core and the Rydberg electron. This condition is expressed by the equation

$$\sum_{i'}\left[\frac{\sin(\pi\nu_i)}{\sqrt{A(\nu_i)}}C_{ii'}+\sqrt{A(\nu_i)}\cos(\pi\nu_i)S_{ii'}\right]B_{i'}=0, \quad (2)$$

where the index i designates a Rydberg channel attached to an ionic state of energy E_i^+ and

$$\nu_i(E)=\left[\frac{\mathcal{R}}{E_i^+-E}\right]^{1/2} \quad (3)$$

represents the effective principal quantum number as a function of the total energy E. $A(\nu_i)$ is Ham's scaling function given in Eq. (2.31) of Ref. [30] and $\mathcal{R}=109\,707.42$ cm^{-1} is the mass-corrected Rydberg constant for H$_2$. The spin-rovibronic quantum defect matrices $C_{ii'}$ and $S_{ii'}$ are defined as

$$C_{ii'}=\int\chi_{v^+}^{(N^+)}(R)\sum_{S\Lambda\Omega}[\langle i^{(sre)}|\alpha^{(sre)}\rangle\cos[\pi\eta_{\ell,\ell'}^{S\Lambda\Omega}(E,R)]$$
$$\times\langle\alpha'^{(sre)}|i'^{(sre)}\rangle]\chi_{v^{+'}}^{(N^{+'})}(R)dR \quad (4)$$

and

$$S_{ii'}=\int\chi_{v^+}^{(N^+)}(R)\sum_{S\Lambda\Omega}[\langle i^{(sre)}|\alpha^{(sre)}\rangle\sin[\pi\eta_{\ell,\ell'}^{S\Lambda\Omega}(E,R)]$$
$$\times\langle\alpha'^{(sre)}|i'^{(sre)}\rangle]\chi_{v^{+'}}^{(N^{+'})}(R)dR, \quad (5)$$

where R is the internuclear distance. These matrices were

evaluated using the procedure described in Ref. [7]. The angular-momentum frame transformation $\langle \alpha'^{(sre)}|i'^{(sre)}\rangle$ between the close-coupling eigenchannels $\alpha^{(sre)}$ and the dissociation channels $i^{(sre)}$ has been defined in Ref. [19]. The superscript (sre) stands for spin, rotation, and electronic angular momenta. This MQDT formalism relies on the explicit definition of only two limiting angular momentum coupling cases $a_{\beta J}$ and e_{exact} (see Ref. [19] for more details). In the following several intermediate coupling cases will be discussed which are implicitly contained in the MQDT framework.

The body-frame quantum-defect functions $\eta_{\ell,\ell'}^{S\Lambda\Omega}(E,R)$ were taken from Ref. [19] without modification and were assumed to be unaffected by interactions with the nuclear spin, which is justified by the weakness of hyperfine interactions compared to electrostatic interactions. Moreover, the very weak dependence of the ion core vibrational wave function $\chi_{v^+}^{(N^+)}$ on the total spin quantum number of the ion G^+ and the total angular momentum quantum number of the ion F^+ has been neglected. The quantum defect functions $\eta_{\ell,\ell'}^{S\Lambda\Omega}(E,R)$ used in the present calculations include all possible $\eta_{p,p}$, $\eta_{f,f}$, and $\eta_{p,f}$ functions, because, although only p levels have been observed, the p and f channels interact with each other as a consequence of the nonspherical symmetry of the ion core.

To treat Rydberg states that lie above the lowest ionization limit, in the so-called autoionizing region of the spectrum, Eq. (2) needs to be adapted. A distinction is made between channels associated with ionic states that lie higher than the total energy of the system and those lying lower than the total energy. The first ensemble of channels is said to be closed and is designated with the letter Q, whereas the second ensemble is said to be open and is represented by the letter P. In this region of the spectrum, the boundary condition requires that the closed-channel wave functions remain finite for $r \to \infty$ and that the open-channel wave functions behave at large r as collision eigenfunctions of the open channels, labeled ρ, with a phase shift τ_ρ. The boundary condition for the closed channels is given by Eq. (2) and that for the open channels by the equations:

$$\sum_{i'} [\sin(\pi\tau_\rho)C_{ii'} - \cos(\pi\tau_\rho)S_{ii'}]B_{i'}^\rho = 0,$$

$$\sum_{i'} [\cos(\pi\tau_\rho)C_{ii'} + \sin(\pi\tau_\rho)S_{ii'}]B_{i'}^\rho = \langle i|\rho\rangle. \quad (6)$$

This set of equations is actually solved in the form of a generalized eigenvalue problem [4]. The elements $\langle i|\rho\rangle$ are normalized according to the requirement

$$\sum_i \langle\rho|i\rangle\langle i|\rho\rangle = 1. \quad (7)$$

In the calculations reported in this article, the vibrational basis has been restricted to $v^+=0$ after having verified that the inclusion of vibrationally excited states does not shift the levels observed in the present work by more than 0.0005 cm^{-1} (including vibrational levels up to $v^+=6$). The

center positions of autoionizing resonances that are narrow compared to their spacings can be predicted by intentionally omitting the open channels. As a result, the same equations are solved as in the case of a bound-state calculation. The shifts resulting from the interaction with the continua have been verified to be insignificant in the present case.

The partial oscillator strength for photoionization into the fragmentation channel $\bar{i}$ is calculated according to

$$\left.\frac{df}{dE}\right|_{\bar{i}} = \frac{2h\nu}{3} \frac{2F'+1}{2F''+1} \left| \sum_\rho \langle\bar{i}|\rho\rangle e^{i\pi\tau_\rho} \sum_i B_i^\rho \sum_\alpha \langle i|\alpha\rangle D_{H,F''}^{\alpha F'} \right|^2, \quad (8)$$

where $\langle i|\alpha\rangle$ denotes the frame transformation $\langle i^{(sre)}|\alpha^{(sre)}\rangle$ introduced above, and $D_{H,F''}^{\alpha F'}$ is the molecule-fixed standing-wave dipole amplitude for the transition from the level F'' of the H state to the component F' of the excited channel α. The total oscillator strength is obtained by summing over all final state channels $\bar{i}$. $D_{H,F''}^{\alpha F'}$ is related to the purely electronic radial transition moments $d_{\ell'\Lambda'}^{\ell\Lambda}(R)$ as spelled out in detail in Eqs. (27)–(29) of Ref. [31] which have been trivially extended to include nuclear in addition to electronic spins. The integration $\int dR \chi_{v^+}^{(N^+)} d_{\ell'\Lambda'}^{\ell\Lambda}(R) \chi_{v^+'}^{(N^{+'})}$ over the vibrational motion is also implied to be included in $D_{H,F''}^{\alpha F'}$. The $d_{\ell'\Lambda'}^{\ell\Lambda}(R)$ refer to specific transitions $\ell' \to \ell$. Since no theoretical predictions of the transition moments from the H state were available to us, we have assumed the H state to be of s character and the transition moments $d_{s\Sigma}^{p\Lambda}(R)$ to be independent of R as well as of the excited state energy E. The values of $d_{s\Sigma}^{p\Sigma}$ and $d_{s\Sigma}^{p\Pi}$ were then adjusted, keeping all other transition moments at zero.

The hyperfine structure in the rotational levels of the ground state of ortho-H$_2^+$ is described by the following effective Hamiltonian [19,32]:

$$\hat{H}_{HFS} = b\vec{I} \cdot \vec{S}^+ + cI_z S_z^+ + d\vec{S}^+ \cdot \vec{N}^+, \quad (9)$$

where $\vec{I}, \vec{S}^+, \vec{N}^+$ are the nuclear spin, core electron spin, and core rotation angular momentum operators, and I_z and S_z^+ are the z components of $\vec{I}$ and $\vec{S}^+$, respectively. The hyperfine-structure constants b, c, and d have been determined experimentally for the $X\,^2\Sigma_g^+$, $v^+=0$, $N^+=1$ level by extrapolation of Rydberg series in Ref. [19], but there are, to our knowledge, neither experimental nor theoretical values of b, c, and d for the $N^+=3$ level of ortho-H$_2^+$. The constants b and c represent the hyperfine interactions between the core-electron and nuclear spins. These constants should therefore, to a first approximation, be independent of the level of rotational excitation, because they only depend on the electronic structure and the magnetic moments of the nuclear spins. The constant d represents the interaction between the core electron spin and rotation and can also be assumed to be independent of the quantum number N^+. We have therefore used the constants b, c, and d determined previously for the $N^+=1$ level and calculated the hyperfine structure in $N^+=3$ for which we have obtained the following eigenvalues and

TABLE II. Calculated case (d) singlet and triplet η quantum defects using the results of Ref. [19] for $R = 2$ a.u.

	$S = 0$	$S = 1$
$np3_2$	$\frac{3}{5}\eta(^1\Sigma_u^+) + \frac{2}{5}\eta(^1\Pi_u^+) = 0.081\,711\,2$	$\frac{3}{5}\eta(^3\Sigma_u^+) + \frac{2}{5}\eta(^3\Pi_u^+) = 0.299\,334\,8$
$np3_3$	$\eta(^1\Pi_u^-) = -0.079\,252$	$\eta(^3\Pi_u^-) = 0.061\,325$
$np3_4$	$\frac{4}{9}\eta(^1\Sigma_u^+) + \frac{5}{9}\eta(^1\Pi_u^+) = 0.039\,98$	$\frac{4}{9}\eta(^3\Sigma_u^+) + \frac{5}{9}\eta(^3\Pi_u^+) = 0.237\,629$

eigenfunctions in the basis $|G^+, F^+\rangle$ of the coupling case $(b_{\beta S^+})$ defined in Ref. [19]

$$\Psi^-(F^+ = 7/2) = -0.999\,097|1/2, 7/2\rangle + 0.042\,493\,0|3/2, 7/2\rangle, \tag{10}$$

$$\Psi^-(F^+ = 5/2) = +0.998\,059|1/2, 5/2\rangle - 0.062\,275\,1|3/2, 5/2\rangle, \tag{11}$$

$$\Psi(F^+ = 3/2) = |3/2, 3/2\rangle, \tag{12}$$

$$\Psi^+(F^+ = 5/2) = -0.062\,275\,1|1/2, 5/2\rangle - 0.998\,059|3/2, 5/2\rangle, \tag{13}$$

$$\Psi^+(F^+ = 7/2) = +0.042\,493\,0|1/2, 7/2\rangle + 0.999\,097|3/2, 7/2\rangle, \tag{14}$$

$$\Psi(F^+ = 9/2) = |3/2, 9/2\rangle, \tag{15}$$

$$E^-(F^+ = 7/2) = -0.031\,582 \text{ cm}^{-1}, \tag{16}$$

$$E^-(F^+ = 5/2) = -0.030\,016 \text{ cm}^{-1}, \tag{17}$$

$$E(F^+ = 3/2) = 0.011\,421 \text{ cm}^{-1}, \tag{18}$$

$$E^+(F^+ = 5/2) = 0.014\,200 \text{ cm}^{-1}, \tag{19}$$

$$E^+(F^+ = 7/2) = 0.016\,433 \text{ cm}^{-1}, \tag{20}$$

$$E(F^+ = 9/2) = 0.017\,040 \text{ cm}^{-1}, \tag{21}$$

where the wave numbers are given with respect to the center of gravity of the hyperfine structure of the $N^+ = 3$ level. These eigenvectors were used in the evaluation of the frame transformation $\langle \alpha'^{(sre)} | i'^{(sre)} \rangle$ according to Eq. (A1) of Ref. [19].

The calculations performed in this study comprise three steps. The first step is an MQDT calculation of the three hyperfine components $F = 2, 3, 4$ of the H ($v = 0, J = 3$) level of H_2 using quantum defect functions for the channels of gerade electronic symmetry obtained from *ab initio* calculations [33]. The second is an MQDT calculation of the high p Rydberg states which is performed either as a continuum calculation, if line shapes are desired, or as a discrete calculation using the closed channels only, if line positions are required. These calculations rely on the quantum defect functions for the channels of ungerade symmetry determined in

Ref. [19]. The last step is the calculation of intensities according to Eq. (8) using R-independent transition moments. The best agreement with the spectra was obtained by using transition moments d_Σ and d_Π of equal magnitude and sign.

The quantum defect functions for the channels of ungerade symmetry have been tested and improved to predict the positions of bound levels around $n = 50$ with an accuracy of 600 kHz [19]. For Rydberg states of gerade symmetry, this level of accuracy has not been reached yet because of additional difficulties caused by interactions with doubly excited configurations of $^1\Sigma_g^+$ symmetry. The hyperfine structure of rovibrational levels of the H state are experimentally unknown and therefore the accuracy of the MQDT predictions of the hyperfine structure of the H state could not be assessed directly. The calculations predict hyperfine splittings in the H ($v = 0, J = 3$) level of less than 30 MHz, which is too small to be resolved in our experiment.

IV. RESULTS

A. Channel structure of H_2 p Rydberg states

Neglecting spin, the channel structure of p Rydberg states of H_2 is well understood [28]. In Hund's case (b), which applies to the lowest members of the p Rydberg series, each state can be assigned a value of Λ of either 0 or 1. For the high-n Rydberg states investigated here, ℓ uncoupling is complete and the Hund's case (b) quantum number Λ is no longer a good quantum number but is replaced by the rotational quantum number N^+ of the ion core. The total angular momentum without spins is then given by $\vec{N} = \vec{N}^+ + \vec{\ell}$, where $\vec{\ell}$ represents the orbital angular momentum of the Rydberg electron. The quantum defects in case (d) can be derived from those in case (b) using the frame transformation $\langle N^+ | \Lambda \rangle$ given in Ref. [28]. The results of this transformation using the quantum defect functions derived in Ref. [19] are given in Table II. Neglecting relativistic effects and interactions with the nuclear spins, the same procedure can be used to define quantum defects for the triplet channels which are also summarized in Table II.

In the present work we have studied autoionizing p Rydberg states of H_2 converging on the rotationally excited level $N^+ = 3$ of the ion. Neglecting all spins there are three p series with different total angular momentum quantum number N that are designated by npN_N^+, i.e., $np3_{2,3,4}$. Since the total angular momentum is conserved in photoionization, only the $np3_2$ series can autoionize at energies between the ionization thresholds corresponding to $N^+ = 1$ and $N^+ = 3$ because the p

continua associated with the $N^+=1$ threshold only comprise $N=0$ to 2. If the pf interaction is taken into account, the $np3_{2,3,4}$ levels can autoionize into the $\epsilon f1_{2,3,4}$ continua. If the spins are considered, the total angular momentum $\vec{F}$ is conserved and the open continua have $F=0$ to 4 which relaxes the restriction mentioned above and opens an ionization channel for some hyperfine components of all three series $np3_{2,3,4}$. In order to assess the importance of these additional pathways for ionization it is necessary to understand the relative importance of the different interactions between angular momenta and their evolution with an increasing level of excitation.

At sufficiently high n values the interactions between the core electron spin and the H_2^+ nuclear spins, which are independent of n, become larger than the exchange interaction between the core and the Rydberg electrons which scales as n^{*-3}, and therefore singlet and triplet levels are mixed. The mixing is almost complete when the singlet-triplet interval becomes equal to or smaller than the largest ionic hyperfine interval. This situation is reached at effective principal quantum numbers of 104, 90, and 101 for the three series $np3_2$, $np3_3$, and $np3_4$, respectively.

To illustrate the gradual evolution of the coupling hierarchy with n, the next subsections describe the level patterns and spectral intensities at selected values of n between 70 and 140. In all figures presented below we have indicated the Hund's case (b) labels of the observed transitions. Although these are not strictly valid labels they enable one to recognize the Kronig's parity and thus assess which states may be subject to predissociation as discussed in Ref. [19].

1. Energy level structure at $n=70$

At $n=70$, the intervals between singlet and triplet levels of $N=2,3,4$ are significantly larger than the ionic hyperfine splittings. Therefore one expects a level structure close to Hund's case (d). Because the H state is a nearly pure singlet state of s character and the total electronic spin is conserved in the absence of interactions with the nuclear spins, one expects to only observe the singlet components of p levels.

Figure 2 shows the photoionization spectrum of ortho-H_2 recorded in the region corresponding to $n\approx70$ from the $H(v=0,J=3)$ level and the results of MQDT calculations of all bound levels (including triplet levels) with $F=1-5$ using Eq. (2), indicated by the symbols above the spectrum. The symbols encode the value of N (crosses for $N=2$, circles for $N=3$, and squares for $N=4$). Rectangular frames have been placed around the final states to which transitions are observed in the spectrum. The spectrum reveals two sharp lines that can immediately be assigned to transitions to the Rydberg states $70p3_4$ and $70p3_3$ using the Hund's case (d) quantum defects given in Table II. The lines consist of several unresolved transitions between the hyperfine components of the H level and the Rydberg states. In addition to the two sharp lines, a broad structure is observed which is assigned to the $70p3_2$ resonance which decays by rotational autoionization into the $\epsilon1_2$ continuum. The width of this structure amounts to 0.075 cm^{-1} corresponding to a reduced width $\Gamma_r = \Gamma n^{*3}$ of 2.6×10^4 cm^{-1}.
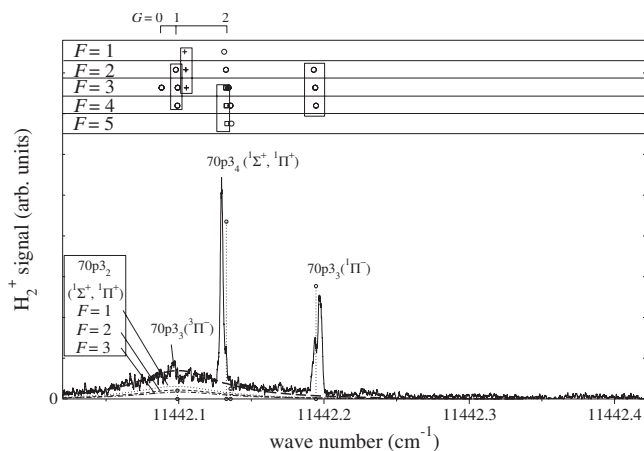

FIG. 2. Photoionization spectrum of ortho-H_2 in the region of $n\approx70$ below the $v^+=0,N^+=3$ ionization limit (solid line) and MQDT calculations of the same spectral region. The results of three different MQDT calculations are shown in the spectrum. These include the result of continuum calculations of the broad $N=2$ resonances using Eq. (6) for $F=1$ (dotted line), $F=2$ (dashed line), $F=3$ (dot-dashed lines), and their sum (thick dashed line), a calculation of positions and intensities of the $F=4$ components using Eq. (2) (vertical lines), and a calculation of all level positions for $F=1-5$ (symbols on top of the figure), including the positions of the $N=2$ resonances. The $np3_2$ levels are marked with crosses, the $np3_3$ levels with circles, and the $np3_4$ levels with squares. The final states that are actually observed in the spectrum are highlighted by rectangular frames and correspond to the singlet components of $70p3_{2,3,4}$. The absolute positions above the $X\ ^1\Sigma_g^+\ (v=0,J=0)$ ground state of H_2 can be derived by adding 113 303.463 cm^{-1} to the wave numbers.

Since the widths of the transitions to the $70p3_4$ and $70p3_3$ states are limited by experimental effects, these transitions are compared to calculations of all bound levels (including triplet levels) with $F=1-5$ using Eq. (2) which are also shown in Fig. 2. The results of a full MQDT calculation of line positions including all spins using Eq. (2) are shown as symbols (see above) in the spectra. For clarity, intensity calculations are presented for the $F=4$ components only (stick spectra) because the singlet components of the autoionizing $np3_2$ resonances have no $F=4$ components and the intensities only weakly depend on F. The natural linewidths of the transitions to the $F=2-4$ components of the $70p3_3$ level and the $F=3-4$ components of the $70p3_4$ levels were calculated from Eq. (6) (not shown) and found to lie in the range between 30 and 270 kHz, well below the experimental resolution.

The analysis of the broad $70p3_2$ resonance requires MQDT calculations using Eq. (6), the result of which is displayed in Fig. 2 for $F=1$ (dotted line), $F=2$ (dashed line), and $F=3$ (dash-dotted line) and is in good agreement with the measured line shapes and positions.

The intensities obtained from bound state calculations and those obtained from continuum calculations can be represented on a common scale by rescaling the calculated resonances so that their integrated intensity corresponds to that obtained from a bound calculation. In this process, which
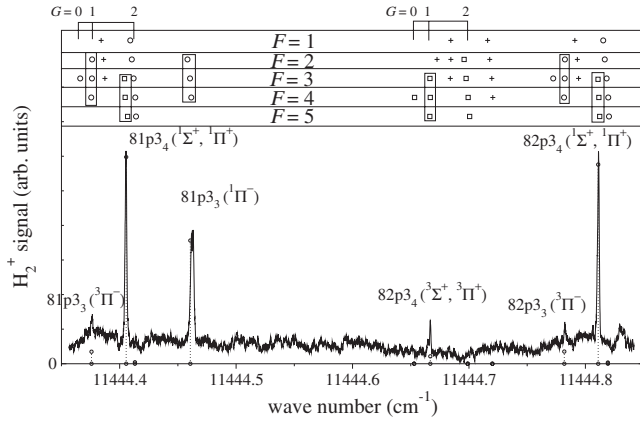
FIG. 3. Photoionization spectrum of ortho-H_2 in the region of $n \approx 80$ below the $v^+ = 0, N^+ = 3$ ionization limit (solid line) and MQDT calculations in the same spectral region. A calculation of positions and intensities of the $F = 4$ components using Eq. (2) (dotted vertical lines) and a calculation of all level positions for $F = 1-5$ are shown. The $np3_2$ levels are marked with crosses, the $np3_3$ levels with circles, and the $np3_4$ levels with squares. The final states that are actually observed in the spectrum are highlighted by rectangular frames. The absolute positions above the $X\ ^1\Sigma_g^+$ ($v = 0, J = 0$) ground state of H_2 can be derived by adding 113 303.463 cm^{-1} to the wave numbers.

amounts to convoluting the calculated profiles with the experimental line shape function, we have used the calculated natural linewidth for the components of the broad $70p3_2$ resonance and the experimentally limited linewidth of 32 MHz or 0.001 cm^{-1} for the sharp transitions. The results of this procedure are shown in Fig. 2 which illustrates the good agreement between calculated and observed linewidths for both bound and continuum calculations.

The finite autoionization linewidths of the $F = 2-4$ components of the $70p3_4$ and $70p3_3$ levels have two different contributions arising from hyperfine interactions and the pf interaction and are discussed in Sec. IV B. The $F = 5$ components can only autoionize if both effects are combined.

The symbols outside the rectangular frames at the top of Fig. 2 correspond to the triplet component of $70p3_3$ that is expected to lie in this region and to produce sharp resonances. A subgroup of transitions to this component is very weakly observed close to the maximum of the $70p3_2$ resonance. The observation of triplet components is a result of the hyperfine interactions in the core as is discussed further below.

2. Energy level structure at $n = 80$

Figure 3 compares the photoionization spectrum recorded in the region corresponding to $n = 81-82$ with the results of an MQDT calculation in the same spectral region. The results of discrete calculations of levels corresponding to $F = 1-5$ are shown as symbols above the spectrum indicating the positions of the different N components and the transitions to $F = 4$ components are shown as stick spectra. The broad resonances corresponding to $N = 2$ cannot be identified unambiguously in this measurement because of an insufficient signal-to-noise ratio.

In the region around $n = 80$, the interval between the singlet and triplet levels is comparable to the hyperfine splitting of the ion. Consequently, neither the total electronic spin quantum number S nor the total core spin quantum number G^+ are good quantum numbers. The spin coupling hierarchy is modified and a new useful angular momentum can be defined, resulting from the coupling between total electronic and total nuclear spin

$$\vec{S} = \vec{S}^+ + \vec{s},$$

$$\vec{G} = \vec{I} + \vec{S},$$

$$\vec{F} = \vec{N} + \vec{G}. \tag{22}$$

The resulting angular momentum coupling case is case (d) to which one adds a total spin angular momentum and is labeled as case ($d_{\beta S}$), indicating that the nuclear spin is coupled to the total electronic spin, according to the nomenclature introduced in Refs. [19,34]. The calculated level pattern can indeed be rationalized using this coupling case and the transitions are labeled by the values of $S, G,$ and N in Fig. 3. The group of levels corresponding to singlet states must have $G = 1$ and therefore F can take the values $N-1, N, N+1$. The triplet levels can be classified into three groups with $G = 0$, which only allows $F = N$, $G = 1$ with $F = N-1, N, N+1$, and $G = 2$ with $F = N-2, N-1, \ldots, N+2$. Of these three groups of levels, the $G = 0$ level always lies lowest in energy and the $G = 2$ levels highest because the eigenvalues of the effective Hamiltonian for the interaction of a total electron spin $\vec{S}$ with a total nuclear spin $\vec{I}$ [which is similar to Eq. (9) excluding the spin-rotation term and with $\vec{S}^+$ replaced by $\vec{S}$] are given by [34]

$$E_{G,S,I} = \frac{1}{6}(3b' + c')[G(G+1) - S(S+1) - I(I+1)], \tag{23}$$

where b' and c' are both positive and close to the values of b and c of the ion core. This result can also be interpreted physically: The opposite signs of the gyromagnetic ratios of proton and electron lead to a preferred antiparallel alignment of the respective spins.

Because of the singlet-triplet mixing induced by the hyperfine interaction the triplet levels gain intensity compared to the situation observed at $n = 70$. However, only a subset of these levels are observed, namely those of the $G = 1$ group. This observation reveals the role of $\vec{G}$ as a conserved quantity since the excitation takes place from a nearly pure singlet level of ortho-H_2 with $G = 1$. This conservation rule actually applies to the whole range of Rydberg states observed in this work, up to $n = 160$, and represents an interesting case of total spin conservation in photoexcitation. The agreement between calculated and measured positions is excellent in this region and the agreement between measured and calculated intensities is satisfactory.
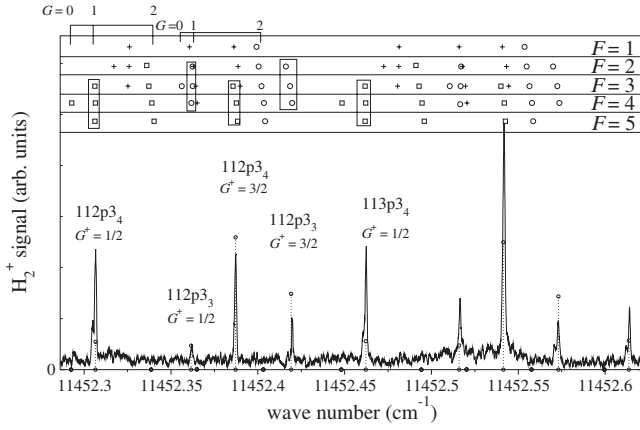
FIG. 4. Photoionization spectrum in the region of $n \approx 111$ (solid line) and MQDT calculations in the same spectral region. See caption of Fig. 3 for further details.

3. Energy level structure at $n = 110$

At $n \approx 110$ the hyperfine splitting in the ion is larger than the singlet-triplet interval for $N = 2, 3, 4$. The level structure starts resembling the ionic structure and can be labeled according to the total spin quantum number of the ion G^+ as can be seen in Fig. 4. The transitions to singlet and triplet levels of $N = 3$ and 4 have nearly equal intensities which shows that singlet-triplet mixing is complete. The corresponding angular momentum coupling situation, while still intermediate, starts approaching the ($d_{\beta S^+}$) limiting case defined by (see also Ref. [35])

$$\vec{G}^+ = \vec{I} + \vec{S}^+,$$

$$\vec{G} = \vec{G}^+ + \vec{s},$$

$$\vec{F} = \vec{G} + \vec{N}. \tag{24}$$

This coupling scheme differs from that encountered in high ℓ ($\ell \geq 3$) states of ortho-H_2 [19,36,37] which can be represented by

$$\vec{G}^+ = \vec{I} + \vec{S}^+,$$

$$\vec{F}_s = \vec{G}^+ + \vec{N},$$

$$\vec{F} = \vec{F}_s + \vec{s}. \tag{25}$$

These two cases can both be described as $d_{\beta S^+}$ but they differ in that the exchange interaction dominates over the spin-rotation interaction in the core in the former case while the opposite is true in the latter.

A continuous transition actually occurs between the limiting cases ($d_{\beta S}$) and ($d_{\beta S^+}$). The transition is described schematically in Fig. 5 which shows on the left-hand side the level diagram appropriate for each $np3_N$ level in case $d_{\beta S}$ [Eq. (22)] and on the right-hand side the level diagram appropriate for the same levels in case $d_{\beta S^+}$ [Eq. (24)]. The good quantum number in this diagram is G as can be seen from Eq. (9) in the case where the spin-rotation term is ne-
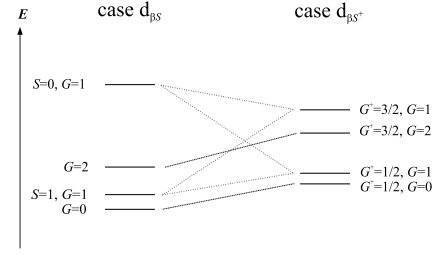

FIG. 5. Correlation diagram illustrating schematically the transition from case $d_{\beta S}$ to case $d_{\beta S^+}$ which occurs when the singlet-triplet interval decreases below the G^+ splitting in the ion. This angular momentum recoupling takes place for each $np3_N$ Rydberg series independently. When the spin-rotation interaction in the ion [the term $d\vec{S}^+ \cdot \vec{N}^+$ in Eq. (9)] is neglected, G remains a good quantum number throughout.

glected. Indeed, the wave function of the molecule can then be written as the product of a $np3_N$ Hund's case (d) wave function without spins and a total spin wave function $|sS^+; SIG\rangle = |S^+I, G^+sG\rangle$. Figure 5 illustrates that the $G = 0$ and 2 components retain triplet character as long as the spin-rotation interaction in the core is negligible and are thus not observable in our experiment. It also shows that the $G = 1$ components which have pure singlet or triplet character at low n values have a completely mixed character at high n. While only one $G = 1$ component corresponding to $S = 0$ is observed at low n (Fig. 2) two are visible at high n (Figs. 3 and 4).

When the last term of Eq. (9) becomes important, G^+ couples to N^+ and the resultant F^+ is a nearly good quantum number. In this situation, G and N have ceased to be good quantum numbers. The dynamical consequences are discussed below in Sec. IV B 1.

The resulting level pattern can be represented schematically as follows:

$$G^+ = 3/2$$

$$[G = 1 \text{ of } S = 0] \, F = N - 1, N, N + 1,$$

$$[G = 2 \text{ of } S = 1] \, F = N - 2, N - 1, N, N + 1, N + 2,$$

$$G^+ = 1/2$$

$$[G = 1 \text{ of } S = 1] \, F = N - 1, N, N + 1,$$

$$[G = 0 \text{ of } S = 1] \, F = N. \tag{26}$$

The observed and calculated spectra shown in Fig. 4 are in good agreement and support the generalized spin conservation rule formulated in Sec. IV A 2.

4. Energy level structure at $n = 140$

At $n = 140$, the Hund's case (d) fine-structure splittings are smaller than the ionic G^+ splitting, such that the spectrum displayed in Fig. 6 is dominated by the G^+ ionic structure. For $N = 3$ the level structure is characteristic of case $d_{\beta S^+}$
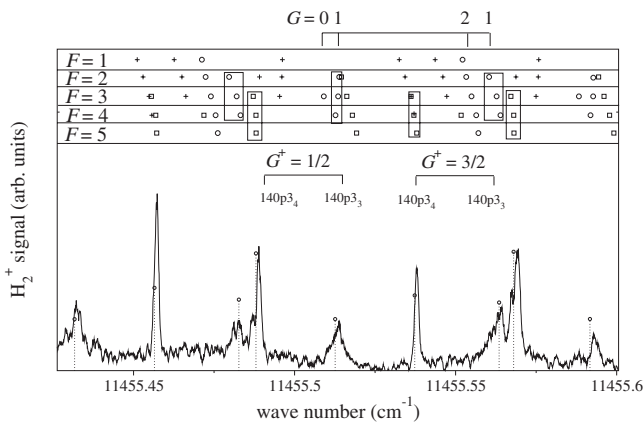
FIG. 6. Photoionization spectrum in the region of $n \approx 140$ (solid line) and MQDT calculations in the same spectral region. See caption of Fig. 3 for further details.

outlined in Eq. (24). The calculations and the spectra show that, within the $G^+=1/2$ manifold, the hyperfine components of the $np3_3$ level with a given G value are shifted to lower energies with increasing F value, whereas the opposite is true for the $G^+=3/2$ manifold. This is interpreted as a signature of the hyperfine structure of the ion core for which an analogous ordering of the F^+ levels within a G^+ manifold is found (see Sec. III). Transitions to the $G=1$ groups of levels are still by far the most intense, confirming the G conservation rule already mentioned above.

5. Correlation diagram

To facilitate the visualization of the evolution of angular momentum coupling hierarchy, a correlation diagram, displayed in Fig. 7, was constructed on the scale of an effective principal quantum number defined with respect to the center of gravity of the hyperfine structure of the $N^+=3$ ionic state. At each n value, the same range of effective principal quantum number (from $n-0.15$ to $n+0.85$) is shown. Figure 7(a) shows photoionization spectra recorded from the $H\ ^1\Sigma_g^+(v=0,J=3)$ level. The results of MQDT calculations solving Eq. (2) for discrete states are displayed in Figs. 6(b) and 6(c), respectively. In these figures the (b) $N=4$ and (c) $N=3$ levels have been connected by lines to guide the eye through the correlation diagram. For clarity, the levels corresponding to $N=2$ have been suppressed because the corresponding resonances are very broad on the scale of the figure and do not reveal any observable hyperfine structure.

This correlation diagram highlights the continuous transition from case $(d_{\beta S})$ (top panel) to case $(d_{\beta S+})$ (bottom panel). The singlet levels $(G=1)$ correlate with the $G^+=3/2$ group of levels and remain closely spaced over the whole range of principal quantum numbers displayed in Fig. 7. The triplet levels can be divided into three groups corresponding to $G=0,1,$ and 2 which evolve differently. The $G=1$ levels [connected by full lines in (b) and (c)] gain intensity over the range $n=80-140$ until they become as intense as the singlet levels. The $G=0$ levels (connected by dotted lines) remain close to the $G=1$ levels originating from the
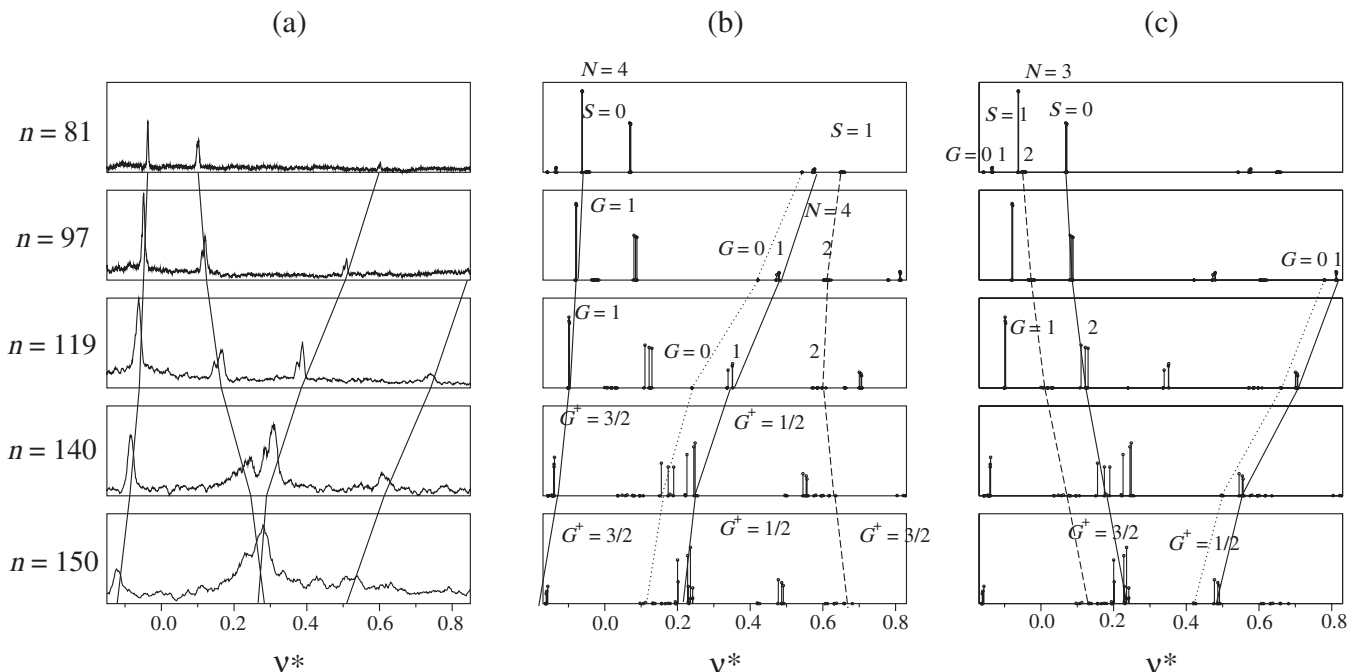

FIG. 7. Comparison of (a) photoionization spectra and (b) and (c) MQDT calculations of the hyperfine structure in the $np3_4$ and $np3_3$ series. The MQDT calculations were performed using Eq. (2) and include intensities for all the transitions from the hyperfine components of the $H(v=0,J=3)$ level to the hyperfine components of the $np3_4$ and $np3_3$ series. The spectra are represented on the scale of an effective quantum number ν^* defined with respect to the center of gravity of the hyperfine components of the $N^+=3$ level of H_2^+. The horizontal scale only gives the fractional value of ν^* with the integer value being given on the left margin for each spectrum. The $G=0,1,$ and 2 levels of (b) $N=4$ and (c) $N=3$ are connected by dotted, full, and dashed lines, respectively.

triplet component and form the $G^+=1/2$ manifold with these levels. The $G=2$ levels (connected by dashed lines) are shifted to higher energies until they merge with the $G=1$ levels originating from the singlet component with which they form the $G^+=3/2$ manifold, at which point the level structure corresponds to Eq. (26) above.

The transitions represented in Fig. 7 connect the $F=2,3,4$ levels of H ($v=0, J=3$) to $np3_N$ levels with $F=N-G,\dots,N+G$. However, only a subset of the transitions allowed by the $\Delta F=0,\pm 1$ selection rule is predicted to carry intensity as is confirmed by the partially resolved structure observed in the experimental spectra. The calculations predict the transitions corresponding to $\Delta F=\Delta N$ to be more intense than the other allowed transitions by more than three orders of magnitude. This propensity can be interpreted as follows: The total spin is conserved in the transitions (i.e., $\Delta G=0$, as discussed above) and is weakly coupled to the other angular momenta, so that the dipole transitions only affect the orbit-rotational part of the wave functions. The relative orientation of $\vec{N}$ and $\vec{G}$ is thus conserved which implies $\Delta F=\Delta N$. This result is expected to have a general validity in transitions between hyperfine components of Rydberg states in Hund's case (d).

The conservation of total spin over the whole range of principal quantum numbers presented here can be understood from the relative strengths of the interactions contained in the effective Hamiltonian given in Eq. (9). If the interactions in the ion core were limited to those between nuclear and core electron spins ($\vec{G}^+=\vec{I}+\vec{S}^+$), G would be a good quantum number up to $n \to \infty$. However, because the core electron spin is coupled to the core rotation, G stops being a good quantum number as soon as this interaction becomes significant, i.e., when the intervals between groups of levels possessing the same value of G become comparable to the splittings in the ionic levels that originate from the interaction term $d\vec{S}^+\cdot\vec{N}^+$. The interaction between nuclear and core electron spins, characterized by the constants b and c, results in a splitting of the ionic level into two G^+ components separated by 0.046 cm^{-1}. The interaction between the core electron spin and core rotation, characterized by the constant $d=0.001\,399(6)$ cm^{-1}, is more than one order of magnitude smaller. Therefore, it is expected that G will remain a good quantum number up to the region $n \approx 170$ where the singlet-triplet interval of the $np3_3$ levels becomes smaller than the largest splitting resulting from the core electron spin-rotation interaction, i.e., the $F^+=9/2-F^+=3/2$ interval of the $N^+=3, G^+=3/2$ manifold. This situation is reminiscent of what happens in series converging to rotationally excited levels of para-H$_2^+$. Series converging on $N^+=0$ can be characterized by a total electron spin quantum number S up to $n \to \infty$. However, the singlet and triplet components of series converging on rotationally excited levels of para-H$_2^+$ will be mixed by the core electron spin-rotation interaction term, but this interaction remains insignificant below $n=170$. In ortho-H$_2$, G plays the same role as S in para-H$_2$: Both are conserved until the exchange interaction becomes less than the spin-rotation interaction, which occurs over a similar range of n values in para- and ortho-H$_2$. For $n>170$, G and N are no longer

conserved and the admixture of $N=2$ character impacts the autoionization of $N=3$ and 4 levels as discussed below.

B. Autoionization dynamics

Only the $np3_2$ levels can autoionize in the absence of spins and when the pf interaction is neglected. This restriction is, however, relaxed if the effects of electron and nuclear spins are considered, because in this case N is no longer a good quantum number and the autoionization of some hyperfine components of the $N=3$ and 4 levels becomes allowed. In the presence of pf interaction, the $np3_3$ and $np3_4$ levels can autoionize into the continua $\epsilon f1_3$ and $\epsilon f1_4$, respectively. In the MQDT calculations, these two effects can be studied separately, the former by including all spins but restricting the calculations to $\ell=1$ and the latter by excluding all spins but including $\ell=1$ and 3 and pf interaction. Since the pf interaction results from short-range effects between the ionic core and the Rydberg electron but the dominant spin interactions are those of the ionic core, one expects that the latter dominate the autoionization dynamics at high n.

The autoionization linewidths presented in this section were determined in calculations which neglected predissociation. It is therefore possible that the actual linewidths of the resonances, which have contributions from predissociation and autoionization, are larger than determined here.

1. Spin-induced rotational autoionization

As can be seen in Fig. 1, open channels in the region investigated here have $F=0-4$ and autoionization is possible for all hyperfine components of $np3_2$, all $G=0$ and $G=1$ components of $np3_3$, the $G=0$ component of $np3_4$, and several $G=1$ and $G=2$ components of $np3_4$. Unfortunately, because of the limited experimental resolution, the spectra have not revealed any broadening of the transitions to $N=3$ and 4 levels that could be attributed to autoionization, which sets an upper limit of approximately 30 MHz for the rate of spin-induced autoionization in these levels. Since the structure and intensity distribution observed experimentally are reproduced satisfactorily by the calculations, it is reasonable to assume that the MQD theory allows quantitative predictions of processes that cannot be seen in our experiment and can be used to explore the role of nuclear and electronic spins in rotational autoionization.

Two regions were investigated in detail. The first corresponds to the region around $n=81$ where the level structure can be described in case (d$_{\beta S}$) and the hyperfine-induced singlet-triplet mixing is weak. Calculated line shapes of the $F=0-5$ resonances are summarized in columns 5 and 6 of Table III. The linewidths were extracted by fitting either a Lorentzian line to the density of states or the Fano line-shape formula [38] to the resonances predicted by MQDT. The hyperfine components of the singlet components of $N=2$ have a width of 0.06 cm^{-1} corresponding to a reduced width of 32 000 cm^{-1}. This large value reflects the fact that rotational autoionization is allowed for these series even in the absence of hyperfine interactions. The triplet components have a reduced width of approximately 80 000 cm^{-1}. The autoionization in the triplet manifold is faster than in the singlet

TABLE III. Linewidths and reduced linewidths of calculated line profiles at $n=81$.

				Without pf interaction		With pf interaction	
N	S	G	F	Γ (cm^{-1})	$\approx\Gamma_r$ (cm^{-1})	Γ (cm^{-1})	$\approx\Gamma_r$ (cm^{-1})
2	0	1	1	0.0612	32 500	0.0612	32 500
			2	0.0604	32 000	0.0604	32 000
			3	0.0604	32 000	0.0604	32 000
2	1	2	0	0.163	87 000	0.163	87 000
			4	0.124	66 000	0.124	66 000
3	0	1	2	1.2×10^{-5}	6.4	1.2×10^{-5}	6.4
			3	4.9×10^{-6}	2.6	4.9×10^{-6}	2.6
			4	8.0×10^{-7}	0.42	8.0×10^{-7}	0.42
4	0	1	3	2.8×10^{-7}	0.15	9.7×10^{-7}	0.52
			4	1.0×10^{-7}	0.05	8.2×10^{-7}	0.44
			5	0	0	7.0×10^{-7}	0.37

TABLE IV. Linewidths and reduced linewidths of calculated line profiles at $n=141$.

				Without pf interaction		With pf interaction	
N	G^+	G	F	Γ (cm^{-1})	$\approx\Gamma_r$ (cm^{-1})	Γ (cm^{-1})	$\approx\Gamma_r$ (cm^{-1})
2	1/2	1	3	0.016	44 000	0.016	44 000
2	3/2	2	0	0.023	64 000	0.023	64 000
			4	0.023	62 000	0.023	62 000
3	1/2	0	3	6.1×10^{-6}	16	6.0×10^{-6}	16
3	1/2	1	2	1.2×10^{-5}	33	1.2×10^{-5}	33
			3	8.7×10^{-6}	24	9.0×10^{-6}	25
			4	5.0×10^{-6}	14	overlapped	
3	3/2	1	2	2.0×10^{-4}	550	overlapped	
			3	2.1×10^{-5}	58	2.2×10^{-6}	60
			4	1.0×10^{-6}	2.7	1.1×10^{-6}	3.0
3	3/2	2	1	1.5×10^{-4}	410	1.5×10^{-4}	410
			2	8.3×10^{-5}	230	8.3×10^{-6}	230
			3	4.2×10^{-5}	110	4.1×10^{-5}	112
			4	2.6×10^{-6}	7	2.8×10^{-6}	8
			5	0	0	$<10^{-8}$	<0.03
4	1/2	0	4	1.3×10^{-7}	0.36	1.3×10^{-7}	0.36
4	1/2	1	3	2.4×10^{-7}	0.67	3.2×10^{-7}	0.90
			4	4.0×10^{-8}	0.11	6.0×10^{-8}	0.17
			5	0	0	7.6×10^{-8}	0.21

manifold of $N=2$ as a result of the larger difference $\left|\eta_{2S+1_\Pi}-\eta_{2S+1_\Sigma}\right|$ [28] in $S=1$ channels compared to $S=0$ channels. In contrast, the reduced widths of the $F=3$ and 4 components of $N=3$ and 4 lie between 0 and 6 cm^{-1}, i.e., are four orders of magnitude less than for $N=2$ because their autoionization is only permitted by hyperfine interactions.

The second region that was investigated in detail lies around $n=141$ and the results are summarized in columns 5 and 6 of Table IV. The reduced linewidth of the $G^+=1/2,F=3$ component of $N=2$, with which the $G=1,F=3$ level correlates at high n, is still very large and has actually increased compared to the situation observed at $n=81$. The singlet-triplet mixing induced by the hyperfine interaction thus manifests itself here as an increased rate of autoionization. The resonances corresponding to $N=3$ and 4 are characterized by a very strong dependence on the quantum numbers N and F. Overall the lifetimes are found to decrease with decreasing values of N and F. This effect can qualitatively be explained by the increasing $N=2$ character of states with low N and F values. The autoionization of the $np3_3$ and $np3_4$ series can thus be considered to result from N mixing induced by the spin-rotation interaction. However, since the autoionization of the $N=2$ levels is still about two orders of magnitude faster, the N mixing must be weak at $n=140$. This result is in accordance with the statement of Sec. IV A 5 that the interactions between the spins conserve G and therefore N. The autoionization rates of the series with $N=2,3$, and 4 will thus only become comparable when N mixing is complete, i.e., at $n>170$, when the spin-rotation splitting in the ion core dominates the level structure. At $n=140$ this mixing is weak. However, because in the absence of any mixing the autoionization lifetimes of the $np3_3$ and $np3_4$ series would be infinite, even a weak mixing leads to the large variation in lifetimes described in Table IV.

2. pf interaction and autoionization

The weak but nonvanishing pf interaction allows p levels to decay into an f continuum with the same value of the total angular momentum quantum number N. For this process, neglecting all spins, we have calculated a reduced natural linewidth of 0.32 cm^{-1} and 0.05 cm^{-1} for the $np3_4$ and $np3_3$ levels lying above the $N^+=1$ threshold, respectively. This contribution to the natural linewidth decreases with n^{*-3} as expected, contributing 31 kHz and 5 kHz to the linewidth of the $70p3_4$ and $70p3_3$ levels, respectively. pf interactions are therefore expected to have a negligible effect at high n values ($n>100$).

The results of MQDT calculations including the hyperfine and the pf interactions are summarized in the last two columns of Tables III and IV for $n=81$ and 141, respectively. At $n=81$, a competition between spin-induced and pf autoionization is found. The effect of pf interactions is directly noticeable in the $N=4$ levels, where the autoionization of the $F=5$ component becomes allowed. The autoionization of the $F=3$ and 4 components is increased by up to one order of magnitude, mostly because the spin-induced autoionization is particularly slow. The reduced linewidths compare well with those expected in the absence of hyperfine interactions. The autoionization of the $F=5$ component is only possible through a combination of spin and pf interactions. For the $N=3$ levels, the spin-induced autoionization is already faster than a possible pf autoionization and the linewidths are independent of the pf interaction. The same applies to the $N=2$ levels, where rotational autoionization dominates over all other processes. At $n=141$, the effect of pf autoionization is completely negligible compared to spin-induced autoionization.

C. Determination of the binding energy of H $(v=0,J=3)$

The analysis of the observed spectra by MQDT enables us to determine, by extrapolation, a more accurate value for the binding energy of the H $^1\Sigma_g^+(v=0,J=3)$ level of H_2 with respect to the center of gravity of the hyperfine structure of the X $^2\Sigma_g^+(v^+=0,N^+=3)$ threshold. The value was obtained in an MQDT fit to the observed transitions and amounts to

$$\frac{E_{\text{ion}}[H\ ^1\Sigma_g^+(v=0,J=3)]}{hc} = 11\,461.144 \pm 0.003 \text{ cm}^{-1}.$$

(27)

The uncertainty in the determination of this value is dominated by the uncertainty in the frequency of the near-infrared radiation (see Table I) with a smaller contribution from the uncertainty in the extrapolation to the series limit. This value can be used to determine a more accurate value for the term value of the H state of $113\,303.463 \pm 0.003$ cm^{-1} using the theoretical value for the ionization energy of H_2 of $124\,417.512$ cm^{-1} [39]. As soon as a more accurate experimental value for this term value becomes available, the present result can be used to determine the ionization energy of H_2 to an accuracy of better than 90 MHz, which would represent a substantial progress over the present accuracy of 400 MHz [40].

Since the H $^1\Sigma_g^+(v=0,J=3)$ level is very nearly a pure singlet level, the hyperfine splittings are expected to be very small and are indeed predicted to amount to ≈ 10 MHz.

V. CONCLUSIONS

We have observed and quantitatively analyzed the evolution of the spin-rovibronic angular momentum coupling hierarchy and the autoionization dynamics in p Rydberg states belonging to series converging on the X $^2\Sigma_g^+(v^+=0,N^+=3)$ level of ortho-H_2^+. At principal quantum numbers below $n=70$, the level structure is represented adequately by Hund's case (d) and a total electron spin quantum number S, which is conserved upon photoexcitation and leads to the observation of singlet levels only. The hyperfine interactions in the ion core lead to a gradual decoupling of the Rydberg electron spin from the core spins which takes place between $n=70$ and $n=150$ and ultimately leads to a level structure that is dominated by the hyperfine splitting of the ion.

The hyperfine-induced singlet-triplet mixing has two main consequences. First, it causes the angular momentum coupling hierarchy to change with principal quantum number and to evolve from the simple case (d) channel structure at $n=70$ to the fully decoupled situation through several intermediate coupling cases, characterized by distinct level patterns and intensities. Second, the mixing has an impact on the autoionization lifetimes of the hyperfine components of the $np3_3$ and $np3_4$ series that results from the admixture of the shorter-lived triplet states.

The spin interactions in the ion core lead to additional mechanisms for rotational autoionization and permit autoionization for some hyperfine components of the $N=3$ and $N=4$ levels. However, the interactions permitting autoionization follow a very strict hierarchy. The autoionization rate of levels that are directly coupled to the continuum by electrostatic interactions ($np3_2$) exceeds that of the other N levels even when the level structure is completely dominated by the hyperfine structure of the ion core; experimentally, only an upper limit of about 30 MHz could be established for the spin-induced rotational autoionization in the range $n<150$. The MQDT calculations have shown that the largest expected linewidths indeed lie below 10 MHz at $n=150$ and have revealed very pronounced propensities for hyperfine interactions. These propensities result in autoionization lifetimes differing by up to four orders of magnitude between the hyperfine components of a given $np3_N$ level. An accurate prediction of the autoionization lifetime of the long-lived Rydberg states ($np3_{3,4}$) can only by reached if the pf interaction is included in the calculation. At low n ($n<70$) the pf interaction determines the autoionization lifetime of the $np3_{3,4}$ levels. At higher values of n, spin-induced autoionization and pf autoionization are in competition but the former completely dominates above $n \approx 100$. The prediction of lifetimes would also need to include predissociation [41], but this is beyond the scope of the present work.

Over the entire range of principal quantum numbers characterized in the present work, up to $n \approx 170$, the observed level patterns and intensity distributions can be explained by the fact that the total spin angular momentum $\vec{G}$ and the total angular momentum without spins $\vec{N}$ are constants of motion as long as spin-rotation effects are negligible. This conservation rule strongly favors transitions with $\Delta F = \Delta N$ and is responsible for the large differences in autoionization rates observed for $N=2$ on the one hand and $N=3,4$ on the other. Beyond $n \approx 170$, these propensity rules are expected to gradually break down as the spin-rotation interaction in H_2^+ induces N mixing.

The spin-induced rotational autoionization investigated in the present work represents a decay pathway that completely dominates over radiative decay. If other pathways of nonradiative decay, like predissociation, are neglected the spin interactions shorten the lifetime of some components by up to five orders of magnitude compared to purely radiative decay. This number is obtained assuming a radiative lifetime of 1 μs for $n=10$ in combination with the n^{*3} scaling law and a spin-induced autoionization linewidth of 5 MHz.

In conclusion, we were able to characterize the role of nuclear and electron spins in the structure and autoionization dynamics of high Rydberg states of ortho-H_2 and to rationalize the observed effects in terms of approximate conservation rules. A worthwhile extension of the present study might involve an excitation scheme starting from a (metastable) triplet state of H_2 which would allow the observation of the $G=0,1$, and 2 levels and test the $\Delta G=0$ conservation rule in the $G=0$ and 2 manifolds.

[1] J. Berkowitz, *Photoabsorption, Photoionization and Photo-electron Spectroscopy* (Academic Press, New York, 1979).

[2] P. M. Dehmer and W. A. Chupka, J. Chem. Phys. **65**, 2243 (1976).

[3] H. Lefebvre-Brion and R. W. Field, *The Spectra and Dynamics of Diatomic Molecules* (Elsevier, Amsterdam, 2004).

[4] C. H. Greene and Ch. Jungen, Adv. At. Mol. Phys. **21**, 51 (1985).

[5] S. Ross and Ch. Jungen, Phys. Rev. Lett. **59**, 1297 (1987).

[6] S. C. Ross and Ch. Jungen, Phys. Rev. A **49**, 4353 (1994).

[7] S. C. Ross and Ch. Jungen, Phys. Rev. A **49**, 4364 (1994).

[8] S. C. Ross and Ch. Jungen, Phys. Rev. A **50**, 4618 (1994).

[9] R. W. Field, C. M. Gittins, N. A. Harris, and Ch. Jungen, J. Chem. Phys. **122**, 184314 (2005).

[10] Ch. Jungen, K. P. Huber, M. Jungen, and G. Stark, J. Chem. Phys. **118**, 4517 (2003).

[11] M. S. Child and Ch. Jungen, J. Chem. Phys. **93**, 7756 (1990).

[12] W. L. Glab *et al.*, J. Chem. Phys. **106**, 5779 (1997).

[13] M. S. Child and W. L. Glab, J. Chem. Phys. **112**, 3754 (2000).

[14] W. Glab and S. T. Pratt, J. Chem. Phys. **120**, 8555 (2004).

[15] E. Mayer and E. R. Grant, J. Chem. Phys. **103**, 10513 (1995).

[16] S. J. Brownbill and T. P. Softley, Mol. Phys. **103**, 2347 (2005).

[17] H. Dickinson, D. Rolland, and T. P. Softley, Philos. Trans. R. Soc. London, Ser. A **355**, 1585 (1997).

[18] H. J. Wörner, U. Hollenstein, and F. Merkt, Phys. Rev. A **68**, 032510 (2003).

[19] A. Osterwalder, A. Wüest, F. Merkt, and Ch. Jungen, J. Chem. Phys. **121**, 11810 (2004).

[20] H. J. Wörner, M. Grütter, E. Vliegen, and F. Merkt, Phys. Rev. A **71**, 052504 (2005).

[21] D. Uy *et al.*, J. Chem. Phys. **113**, 10143 (2000).

[22] M. Schäfer and F. Merkt, Phys. Rev. A **74**, 062506 (2006).

[23] R. Seiler, Th. Paul, M. Andrist, and F. Merkt, Rev. Sci. Instrum. **76**, 103103 (2005).

[24] Th. A. Paul and F. Merkt, J. Phys. B **38**, 4145 (2005).

[25] K. Tsukiyama, J. Ishii, and T. Kasuya, J. Chem. Phys. **92**, 875 (1992).

[26] D. Dziczek, J. M. Ajello, G. K. James, and D. L. Hansen, Phys. Rev. A **61**, 064702 (2000).

[27] E. Riedle, S. H. Ashworth, J. T. Farrell, Jr., and D. J. Nesbitt, Rev. Sci. Instrum. **65**, 42 (1994).

[28] G. Herzberg and Ch. Jungen, J. Mol. Spectrosc. **41**, 425 (1972).

[29] A. Osterwalder and F. Merkt, Phys. Rev. Lett. **82**, 1831 (1999).

[30] M. J. Seaton, Rep. Prog. Phys. **46**, 167 (1983).

[31] Ch. Jungen and G. Raseev, Phys. Rev. A **57**, 2407 (1998).

[32] K. B. Jefferts, Phys. Rev. Lett. **23**, 1476 (1969).

[33] H. J. Wörner, Ch. Jungen, M. Telmini, and H. Oueslati (unpublished).

[34] R. A. Frosch and H. M. Foley, Phys. Rev. **88**, 1337 (1952).

[35] A. Osterwalder, Ph.D. thesis, ETH Zürich, Diss. ETH Nr. 14551 (2002) (unpublished).

[36] P. W. Arcuni, E. A. Hessels, and S. R. Lundeen, Phys. Rev. A **41**, 3648 (1990).

[37] Z. W. Fu, E. A. Hessels, and S. R. Lundeen, Phys. Rev. A **46**, R5313 (1992).

[38] U. Fano, Phys. Rev. **124**, 1866 (1961).

[39] W. Kołos, K. Szalewicz, and H. J. Monkhorst, J. Chem. Phys. **84**, 3278 (1986).

[40] A. de Lange, E. Reinhold, and W. Ubachs, Phys. Rev. A **65**, 064501 (2002).

[41] Ch. Jungen and S. C. Ross, Phys. Rev. A **55**, R2503 (1997).